Measurement 132 (2019) 263–271

Contents lists available at ScienceDirect

Measurement

journal homepage: www.elsevier.com/locate/measurement

Uncertainty analysis applied to electrical components diagnosis by infrared thermography

R.A.M. Ferreira [a], B.P.A. Silva [a], G.G.D. Teixeira [a], R.M. Andrade [a], M.P. Porto [a,b]

[a] Laboratório de Termometria do Departamento de Engenharia Mecânica da UFMG, Programa de Pós Graduação em Engenharia Mecânica, Universidade Federal de Minas Gerais, Belo Horizonte, MG, Brazil
[b] Bolsista do CNPq (303861/2017-7), Brazil

ARTICLE INFO

Article history:
Received 31 July 2018
Accepted 13 September 2018
Available online 21 September 2018

Keywords:
Infrared thermography
Measurement uncertainty
Monte Carlo Method
GUM

ABSTRACT

This work presents a discussion on the use of infrared thermography to detect degradation of electrical components, highlighting the importance of uncertainty analysis into decision making process. Some technical standards recommend to use temperature differences between similar components as an integrity indicative (a comparative approach). Temperature measurement from infrared cameras is dependent of target surface emissivity and environmental conditions, which impact the measurement accuracy and lead comparative approaches to inconclusive results. We make laboratory experiments under controlled conditions to demonstrate how emissivity affects the temperature uncertainty. We also performed a thermographic inspection using NETA MTS-2011 for an electrical substation connector and discuss the influence that temperature uncertainty has on recommended actions suggested by this standard. Uncertainty was determined using the Guide to the Expression of Uncertainty in Measurement (GUM) and the Monte Carlo Method (MCM). We concluded that uncertainty measurement analysis of thermographic inspections is a crucial step on preventive maintenance of electrical components.

1. Introduction

Thermography has a wide application in detecting degradation of electrical components in substations. This is because electrical deterioration is manifested in terms of temperature increase, and thermal images are useful to identify hot spots. Thermography has improved the efficiency on maintenance of electrical installations, allowing long distances inspections without physical contact (safety) and not requiring any equipment shutdown (no production loss).

But, temperature measured by itself is not a self indicative of the components condition, since the environmental variations (wind velocity, irradiance, humidity, etc.) have direct influence on the thermodynamic equilibrium. In this context, some methods propose to use temperature difference between similar objects in the same scene as an integrity criterion. In these methods, the selected objects are placed in the same thermal image frame, where one component is the reference and the other is under evaluation. In other technical recommendations, temperature difference between the component and environment is used as integrity criterion. Technical standard NETA MTS-2011 [1] suggests exactly these both alternatives and recommends predetermined actions for each given temperature difference interval, as can be seen in Table 1.

In some situations, thermographers develop their own tables based on their experience in a particular substation or component looking for more reliable results. However, there is no scientific guarantee of results obtained without an appropriate uncertainty analysis [2].

Thermography technique has been applied for different areas of engineering [3–7], and methods to estimate uncertainty in thermal images are well established [8–11]. In case of electrical components failure detection, studies on thermography can also be found in the literature [12–14], including smart monitoring systems [15,16]. However, none of them presents an uncertainty analysis, nor highlight its importance to diagnosis evaluation and in the decision making process.

Looking to fill out this gap, in this paper we present a methodology based on GUM and Monte Carlo Method (MCM) to estimate the temperature uncertainty of electrical components, highlighting the influence of target surface emissivity on results.

https://doi.org/10.1016/j.measurement.2018.09.036
0263-2241/

Nomenclature

c	sensitivity coefficient
d	distance, m
d_{high}	absolute difference of upper limits of GUM and MCM coverage intervals
d_{low}	absolute difference of lower limits of GUM and MCM coverage intervals
DTR	digital temperature resolution
$g(x_i)$	probability density function of variable x_i
k_p	coverage factor
M	number of random values generated in MCM
ME	minimum error
MSR	measurement spatial resolution
MU	measurement uniformity
n	number of measurand observations
N	number of input variables in f model
NGE	noise generated error
r	correlation coefficient
R	electrical resistance, $\mu\Omega$
RE	repeatability
s	standard deviation
S	detector signal, W m^{-2}
STRF	slit temperature response function
t_p	Student's t-distribution factor
Δt_{NETD}	thermal resolution, K
$\Delta\widehat{T}$	average temperature difference, K
T	temperature, K
TS	temperature stability
ΔT	temperature difference, K
u	standard uncertainty
u_c	combined standard uncertainty
U	expanded uncertainty
ν_{eff}	degrees of freedom
x_i	input variable i estimated value
X_i	input variable i true value
y	output variable estimated value
Y	output variable true value
$\hat{y}$	output variable average value

Greek

δt	sensitivity for a non-uniform FOV, K
ε	emissivity
η_i	output variable random value
ξ_i	input variable random value
τ	atmospheric transmissivity

Subscripts

amb	ambient
atm	atmospheric
C1	degraded connector
C2	new connector
intr	intrinsic source
max	coverage interval upper limit
min	coverage interval lower limit
ob	object
p	confidence level
p_1,p_2	suspect point reading
ref	reference
refl	reflected

Table 1
Criteria and recommended actions by NETA MTS-2011 [1].

ΔT	ΔT_{amb}	Recommended action
1 °C–3 °C	1 °C–10 °C	Possible deficiency; warrants investigation.
4 °C–15 °C	11 °C–20 °C	Indicates probable deficiency; repair as time permits.
–	21 °C–40 °C	Monitor until corrective measures can be accomplished.
>15 °C	>40 °C	Major discrepancy; replace immediately.

2. Temperature measurement by thermography

During a thermographic inspection, the radiation captured by the imager lenses is comprised of three parts. The mathematical relation to describe the radiation absorbed by infrared sensors (S) is given by Eq. (1) [17]

$$S = \varepsilon\tau S_{ob} + \tau(1-\varepsilon)S_{refl} + (1-\tau)S_{atm}, \quad (1)$$

where ε is the object emissivity and τ is the atmosphere transmissivity between the target's surface and detector. S_{ob}, S_{ref} and S_{atm} are the detectors input signals corresponding to the object, reflected and ambient temperatures. Fig. 1 depicts all signals that compound a inspection scenario from an object with emissivity, ε, and temperature T_{ob} located at a distance d of an infrared camera. Then, the imager converts all radiation inputs into an estimated value of object temperature.

Atmospheric transmissivity can be considered a function dependent of the object distance, with no representative loss of accuracy. So, we conclude that the object temperature can be generally represented as

$$T_{ob} = f(\varepsilon, d, T_{refl}, T_{atm}, S). \quad (2)$$

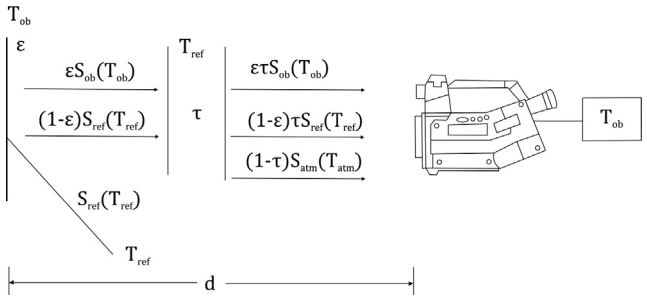

Fig. 1. Schematic view of temperature measurement with a thermal imaging camera [17].

3. Measurement uncertainty

3.1. GUM method

Guide to the Expression of Uncertainty in Measurement (GUM) [18] divides uncertainties into two categories, Type A and Type B.

Type A is obtained from standard deviation, s, which is estimated from a series of measurand readings. Type B evaluation is characterized by choosing the best probability density function (pdf) to represent the measurements [18]. Both uncertainty types obey probability distributions, and can be evaluated by statistical methods.

In case of an indirect measurement, the output true value Y is determined using input true values X_i into the mathematical relation

$$Y = f(X_1, X_2, \ldots, X_N). \quad (3)$$

X_i values are not practical to obtain due to the limited accuracy of instruments, thus estimated values x_i are used into Eq. 3 to estimate the output y

$$y = f(x_1, x_2, \ldots, x_N), \tag{4}$$

where each x_i is associated to a standard uncertainty $u(x_1), u(x_2), \ldots, u(x_N)$ defined as Type A or Type B. The combined standard uncertainty $u_c(y)$ is estimated by the Uncertainty Propagation Law, Eq. (5) [19]. A schematic representation of GUM procedure is depicted in Fig. 2.

$$u_c^2(y) = \sum_{i=1}^{N} c_i^2 u^2(x_i) + \sum_{i=1}^{N-1} \sum_{j=i+1}^{N} c_i c_j u(x_i) u(x_j) r(x_i, x_j). \tag{5}$$

After determining the combined standard uncertainty, the expanded uncertainty, U_p, can be calculated by the product $U_p = k_p u_c(y)$ where k_p is a coverage factor. Expanded uncertainty is the range in which the measured value is expected to be, for a confidence level p. Therefore, the measurement result is expressed by

$$Y = y \pm U_p. \tag{6}$$

The coverage factor k_p that achieves the level of confidence p is obtained by assuming the approximation $k_p = t_p(\nu_{eff})$ where $t_p(\nu_{eff})$ is a factor derived from Student's t-distribution with effective degrees of freedom ν_{eff}, calculated by the equation of Welch-Satterthwaite [19]

$$\nu_{eff} = \frac{u_c^4(y)}{\sum_{i=1}^{N} \frac{u_i^4(y)}{\nu_i}}, \tag{7}$$

and the expanded uncertainty is

$$U_p = t_p(\nu_{eff}) u_c(y). \tag{8}$$

3.2. Monte Carlo Method

Monte Carlo Method (MCM) is a class of numerical approaches that uses random numbers to support statistical analysis [20]. MCM is considered one of the simplest methods to solve uncertainty problems in a probabilistic framework [21], and is an alternative when the mathematical model is complex or does not meet GUM required application criteria [22].

As can be seen in Fig. 3, a probability density function g_{xi} is defined for each one of the N input variables that comprises the mathematical model $Y = f(X_1, X_2, \ldots, X_N)$. Then, a large number M of random values ξ_i is generated for each input variable, obeying the probability distributions previously assumed. M sets of random inputs are simultaneously evaluated by the f model, producing M results η_i used to obtain statistical properties and estimate the probability density function g_Y of the output variable Y.

Numerical results of Y are used to determine the average value $\widehat{y}$, standard uncertainty $u(\widehat{y})$, and coverage interval $[y_{min}, y_{max}]$, which is based on the desired confidence level p. The average value $\widehat{y}$, for M results ordered by y_r and $r = 1, \ldots, M$, is given by

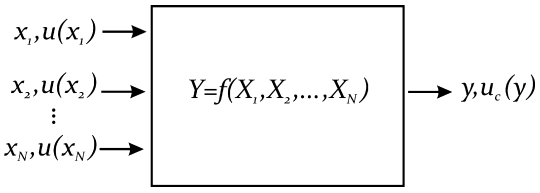

Fig. 2. Schematic diagram representing GUM method to estimate measurement uncertainty [19].

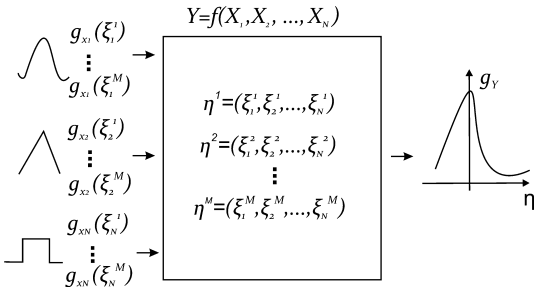

Fig. 3. Schematic diagram representing the Monte Carlo Method to estimate measurement uncertainty [19].

$$\widehat{y} = \frac{1}{M} \sum_{r=1}^{M} y_r, \tag{9}$$

and the standard uncertainty is

$$u(y) = \sqrt{\frac{1}{M-1} \sum_{r=1}^{M} (y_r - \widehat{y})^2}. \tag{10}$$

To generate the pseudo-random numbers, we used the Linear Congruential Method [23], which is able to generate a sequence of numbers with uniform distribution within the range from 0 to 1. Basically, this is a recursive method that starts from an initial number X_0, called seed, and all following numbers given by

$$\begin{aligned} X_{i+1} &= (aX_i + b) \bmod m, \\ R_i &= X_i / m, \end{aligned} \tag{11}$$

where a is a constant, b an increment, and m the modulus of the recursive method. The current normalized element in the generated random sequence is represented by R_i.

3.3. Validation

The Joint Committee for Guides in Metrology (JCGM) [22] recommends to compare results from GUM and MCM through Eq. 12

$$\begin{aligned} d_{low} &= |(y - U_p) - y_{min}|, \\ d_{high} &= |(y + U_p) - y_{max}|. \end{aligned} \tag{12}$$

Absolute differences between interval d_{low} and d_{high} must not exceed a predetermined tolerance, δ. Values of δ are based on a reference significant digit n_d given by the expression of the combined standard uncertainty. In this paper is assumed a value of $\delta = 0.5$ K, applicable in temperature measurements, according to the recommendations of [22].

3.4. Sources of measurement uncertainty

Sources of measurement uncertainty are divided into intrinsic (see Fig. 4), related to the infrared camera internal components, and extrinsic, due to the environmental conditions and measurand.

Thermal imager are calibrated under a controlled room temperature, which means that the camera sensors are maintained under the same temperature along all calibration process. On the other hand, during the thermographic inspections the ambient temperature is usually not the same, and sensors operate out of the calibration condition, affecting the result [24]. Temperature Stability (TS) estimates the influence of ambient temperature on the camera sensors. The distribution used to represent this intrinsic uncertainty is the uniform distribution, given by

$$u_{TS}\left(\widehat{T}_{ob}\right) = \frac{TS}{\sqrt{12}}. \tag{13}$$

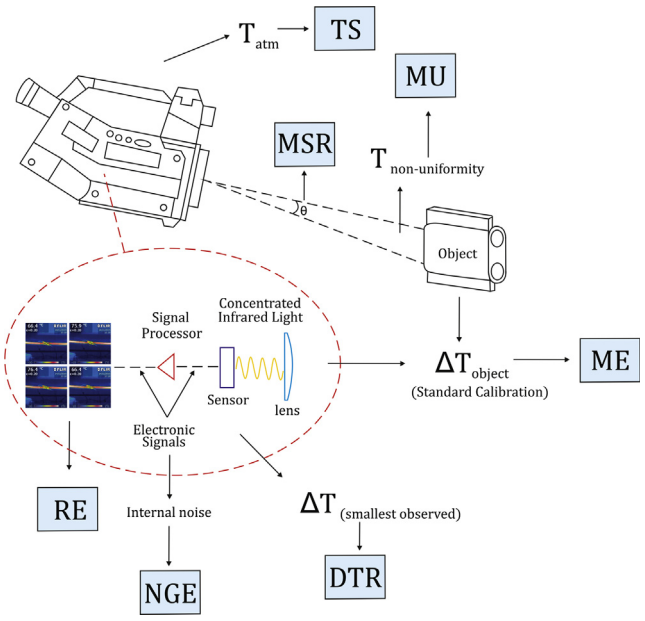

Fig. 4. Intrinsic sources of uncertainty during a thermographic inspection: Temperature Stability (TS), Repeatability (RE), Digital Temperature Resolution (DTR), Minimum Error (ME), Measurement Spatial Resolution (MSR), Measurement Uniformity (MU), and Noise Generated Error (NGE).

Measurement Spatial Resolution (MSR) is defined as the minimum angular dimension of the measurand that produces some influence on the temperature measurement result [24]. MSR can be estimated using the procedure depicted in Fig. 5 (*a*), consisting on the observation of a blackbody source through a vertical slit. MSR is proportional to the angular slit dimension ($\alpha = l/R$) for which the Slit Temperature Response Function (STRF) is 0.99 [24]

$$STRF = \frac{T_{slit} - T_{amb}}{max(T_{slit} - T_{amb})}. \tag{14}$$

The uncertainty due to the MSR is often neglected because the angular size of the measurand is in most cases greater than the angular slit dimension α.

Measurement Uniformity (MU) estimates the range for all measurement results in different measurand positions within the field of view (FOV) of the thermal imager [24], as observed in Fig. 5 (*b*). This uncertainty is estimated by a thermal imager parameter defined as sensitivity to a nonuniform field of view δt

$$\delta t = \widehat{T}_{max} - \widehat{T}_{min}, \tag{15}$$

where $\widehat{T}_{max}$ and $\widehat{T}_{min}$ are the maximum and minimum mean temperatures obtained in each area of the thermogram, respectively. The best estimation of MU is given as an uniform distribution where $MU = \delta t$

$$u_{MU}\left(\widehat{T}_{ob}\right) = \frac{MU}{\sqrt{12}}. \tag{16}$$

Noise Generated Error (NGE) is defined as the temperature standard deviation due to internal noise, and is estimated based on the NETD (Noise Equivalent Temperature Difference), also known as thermal resolution, which is obtained using a blackbody source [25].

$$\Delta t_{NETD} = \frac{\sqrt{2}}{2}\sqrt{\sum_{i=1}^{X}\sum_{j=1}^{Y}\frac{\left(\Delta T_{ij} - \Delta\widehat{T}\right)^2}{HV}}, \tag{17}$$

where ΔT_{ij} is the temperature difference between consecutive thermograms at the same position (i,j), and $\Delta\widehat{T}$ represents the average among all temperature differences. H and V are the pixels number in horizontal and vertical directions, respectively.

In case of $\Delta t_{NETD} = NGE$

$$u_{NGE}\left(\widehat{T}_{ob}\right) = \Delta t_{NETD}. \tag{18}$$

Minimum Error (ME) uncertainty is estimated using a calibrated blackbody source in a similar configuration as depicted in Fig. 5 (*c*), and is defined as the dispersion of the measured value T_{ob} in respect to the true value T_{actual} [24]. The contribution of ME is also given by an uniform distribution

$$u_{ME}\left(\widehat{T}_{ob}\right) = \frac{\widehat{ME}}{\sqrt{12}}, \tag{19}$$

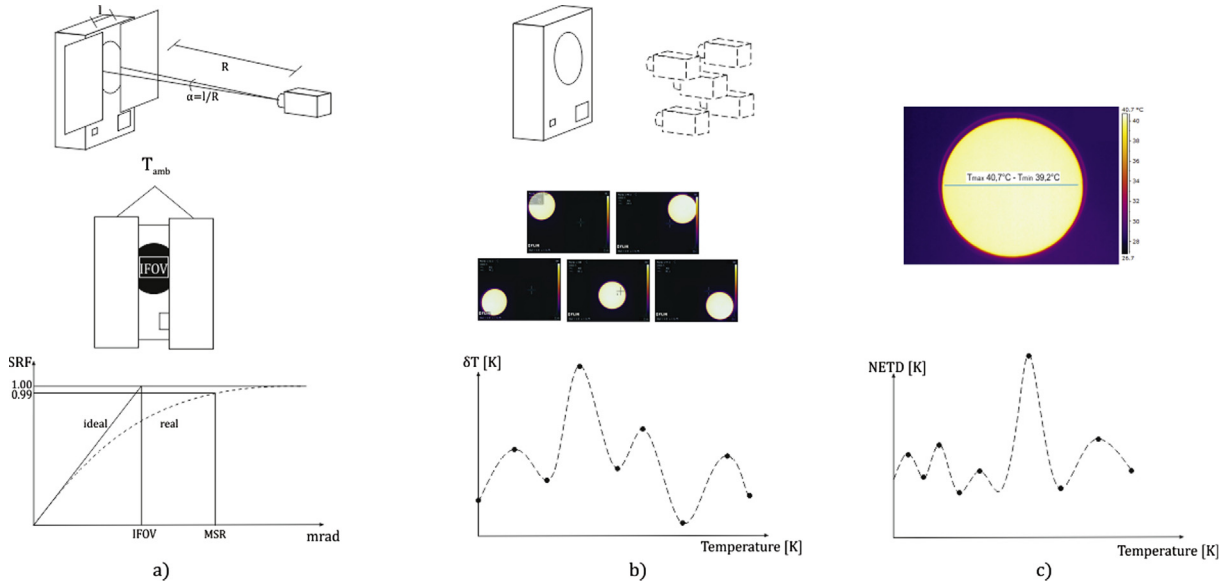

Fig. 5. Methods to estimate intrinsic sources of measurement uncertainty using a blackbody source: a) MSR b) MU and c) NGE.

$$\widehat{ME} = \frac{1}{n}\sum_{i=1}^{n} ME_i,$$
$$ME_i = |\widehat{T}_{actual,i} - \widehat{T}_{ob,i}|. \tag{20}$$

Repeatability (RE) is determined from the mean experimental standard deviation $s_{RE}\left(\widehat{T}_{ob}\right)$, using a similar procedure as shown in Fig. 5(c), by taking n observations of the object temperature T_{ob}

$$s_{RE}(T_{ob}) = \sqrt{\frac{1}{n-1}\sum_{k=1}^{n}\left(T_{ob,k} - \widehat{T}_{ob}\right)^2},$$
$$u_{RE}\left(\widehat{T}_{ob}\right) = \frac{s_{RE}(T_{ob})}{\sqrt{n}}. \tag{21}$$

Digital Temperature Resolution (DTR) is a source of uncertainty that accounts for the influence of limited resolution of digital channels on the minimum temperature difference that can be observed. DTR value can be estimated by [24]

$$DTR = \frac{\Delta T_{span}}{2^k}, \tag{22}$$

where k is the bits number of the analog-digital converter, and ΔT_{span} is the nominal temperature range of the camera. DTR distribution is assumed as uniform

$$u_{DTR}\left(\widehat{T}_{ob}\right) = \frac{DTR}{\sqrt{12}}. \tag{23}$$

Extrinsic uncertainty sources are due to emissivity, distance, reflected temperature and atmospheric temperature.

Emissivity can be estimated by basically two comparative approaches: using a known emissivity coating or tape, or with a calibrated thermocouple. The first technique consists on applying a high emissivity coating in a small portion of the surface. The high emissivity region can be used to determine the temperature accurately. As long as the temperature is the same all over the body surface, we can target at the non-coated region adjusting the emissivity until the temperature be the same. The second approach is quite similar and consists on adjusting the emissivity until the temperature observed by a thermal imager be the same as the one measured by a thermocouple, assumed as reference. Applying one of the aforementioned techniques to several points of the target surface is possible to obtain statistical properties of emissivity, as the mean and standard deviation values, also to estimate the probability density function of this variable.

Variables d, T_{refl} e T_{atm} are measured for each one experiment made. The reflected temperature is assumed as the same as the ambient temperature, which was obtained from a meteorological data acquisition system.

4. Methodology

4.1. Experimental procedure

Emissivity has a direct influence in a radiometric measurement. So, variations in the surface condition may lead to temperature readings completely different during a thermographic inspection in electrical components. In addition, weather conditions and measurand-dependent variables also need to be known in order to obtain a reliable diagnostic for an identified thermal anomaly.

During an outdoor thermographic inspection is difficult to separate all uncertainty components, mainly due to weather variability (wind, humidity and solar irradiation), then first we decide to make steady-state experiments in laboratory to understand the indoor effects first [26].

As part of laboratory tests, we built a test bench comprised of an AC current source, aluminum cables, connectors (used alternately two H type connectors, see Fig. 6), a scientific infrared camera, K-type thermocouples connected to a data acquisition system, a microohmmeter to verify electrical resistance of the samples and a meteorological data acquisition system to measure ambient conditions, as described in Table 2 (Fig. 7).

The selected H-type connectors (namely C1 and C2) have initial resistances $R_{C1} = 199\ \mu\Omega$ and $R_{C2} = 85\ \mu\Omega$ and emissivities of 0.13 and 0.12, respectively. The difference between both samples is that C1 is degraded, which can be confirmed by the high value of electrical resistance, whereas C2 is new, and it was not used before the

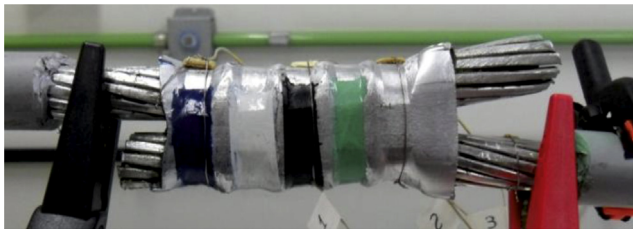

a) Connector C1

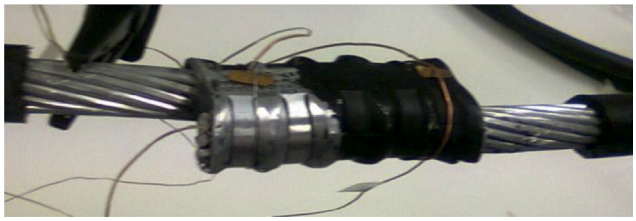

b) Connector C2

Fig. 6. H-type electrical connectors used during the experiments.

Table 2
Instruments specification for the experimental test bench.

Instrument	Commercial model
AC current source	SMC LET-1000-RD
Infrared camera	Flir SC660
Data acquisition system	Agilent 34970A
Microohmmter	Instrum MICROHM-10
Scientific ambient monitor	TESTO 622

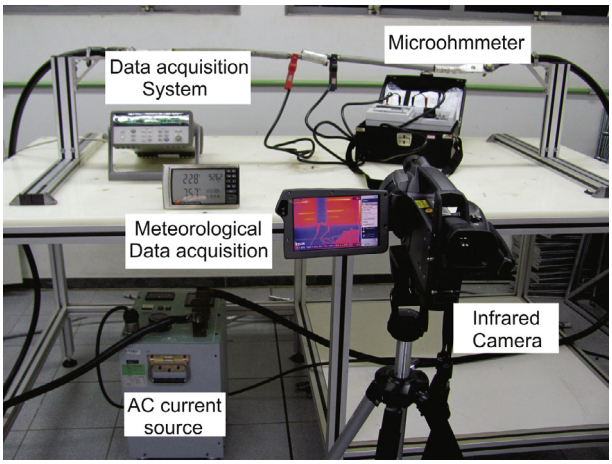

Fig. 7. Experimental test bench built to make thermographic analysis of electrical components.

experiments we have made. To determine the emissivity experimentally, connectors C1 and C2 surfaces were partially covered with a commercial coating, with $\varepsilon = 0.97$.

To perform the experiments in laboratory, we take the following steps:

1. install the selected connector, C1 or C2;
2. measure the electrical resistance of the connector;
3. attach the thermocouples on the sample;
4. start the data acquisition system;
5. adjust the electrical current as 150 A;
6. record the environmental conditions;
7. monitor the steady-state by the thermocouples readings;
8. use the infrared camera to register thermograms (in the coated and non-coated areas);
9. adjust the electrical current for 50 A higher and return to step 6; 500 A is the maximum current evaluated.

We repeat the aforementioned procedure for both H-type connectors. For all measurements, the camera was positioned 30° out of normal direction to avoid the influence of reflected radiation from the thermographer into the results [27].

4.2. Measurement uncertainties

In this section we present GUM and MCM assumptions to estimate the combined standard uncertainty of the temperature measurements.

4.2.1. GUM assumptions

Eq. (5) presents the uncertainty sources that comprise the mathematical relation of the combined standard uncertainty. Including the intrinsic and extrinsic uncertainties of a thermographic measurement and simplifying Eq. (5), we obtain

$$u_c^2(T_{ob}) = c_\varepsilon^2 u_\varepsilon^2 + c_d^2 u_d^2 + c_{T_{refl}}^2 u_{T_{refl}}^2 + c_{T_{atm}}^2 u_{T_{atm}}^2 + u_{intr}^2. \quad (24)$$

In Eq. (24), all variables were considered non-correlated. The uncertainty component u_{intr} comes from the combined intrinsic uncertainties discussed in Section 3.4, and is determined by Eq. (25)

$$u_{intr} = \sqrt{u_{NGE}^2 + u_{TS}^2 + u_{RE}^2 + u_{DTR}^2 + u_{ME}^2 + u_{MU}^2 + u_{MSR}^2}. \quad (25)$$

Table 3 presents the probability distributions we assume for all the uncertainties sources.

4.2.2. MCM assumptions

In this work, the probability density function of emissivity was obtained experimentally by comparison using the contact temperature method. Fig. 8 presents the histogram obtained from a set of 50 measurements along the surfaces of both H-type connectors

Table 3
Probability distribution functions assumed during GUM evaluation.

Uncertainty Sources	Distribution
Emissivity, ε	Uniform
Target Distance, d	Uniform
Reflected Temperature, T_{refl}	Uniform
Atmospheric Temperature, T_{atm}	Uniform
Noise Generated Error, NGE	Uniform
Temperature Stability, TS	–
Measurement Repeatability, RE	Normal
Digital Temperature Resolution, DTR	Uniform
Minimum Error, ME	Uniform
Measurement Spatial Resolution, MSR	–
Measurement Uniformity, MU	Uniform

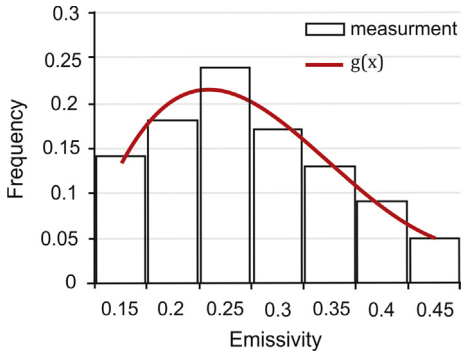

Fig. 8. Histogram of emissivity measurements, and the probability distribution function associated.

used in the experiments and its respective *pdf* estimated by polynomial interpolation.

To generate a sequence of random numbers that obey the *pdf*, we limit the range of possible values that the emissivity can assume along the numerical simulation between 0.15 and 0.45.

With the set of possible values and associated probabilities given by $g(x)$ function, the next step is to perform successive tests using the Linear Congruential Method (LCM) to include random numbers at the list being generated. The advantage of this procedure lies in the use of a random number generator (as LCM), that essentially provides a rectangular distribution, to generate random numbers that obey a generic *pdf*.

Fig. 9 shows a histogram of generated values, provided with the aforementioned algorithm, compared to a histogram of experimental values. In this case, we observed a deviation less than 3% between numerical and experimental results.

Table 4 shows all assumed distributions, in case of MCM. Only variables those were presented on Eq. (2) received an associated *pdf*, also the digital signal S, which involves all intrinsic uncertainties.

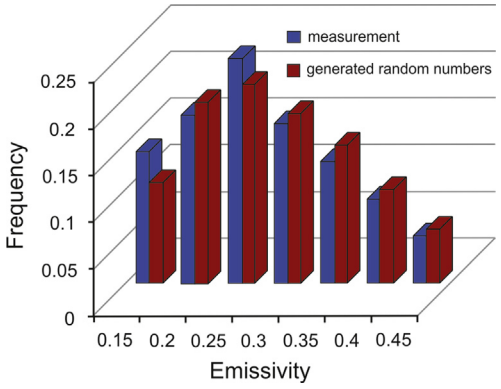

Fig. 9. Comparison between experimental and simulated values of emissivity; the latter is provided from a routine developed to randomly generate emissivity values obeying the probability density function $g(x)$.

Table 4
Assumed probability distributions for the MCM.

Uncertainty Sources	Distribution
Emissivity, ε	$g(x)$
Target Distance, d	Uniform
Reflected Temperature, T_{refl}	Uniform
Atmospheric Temperature, T_{atm}	Uniform
Digital Signal, S	Normal

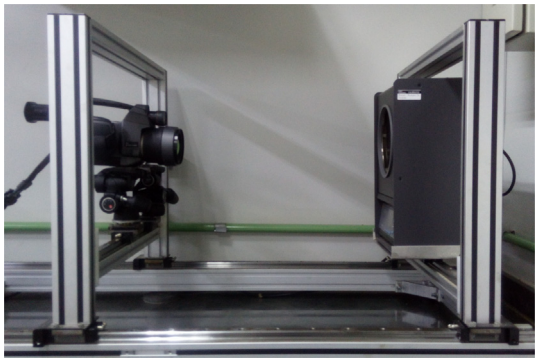

Fig. 10. Intrinsic uncertainty test bench, using a blackbody source Fluke 4181.

4.2.3. General assumptions

In this work, the angular dimension of all analyzed objects is larger than MSR. Thus the influence of MSR on measurement uncertainty was neglected. TS was considered negligible as well. DTR was estimated by the temperature range of Flir SC660 and all the other sources of intrinsic uncertainty were experimentally estimated in laboratory using a blackbody source Fluke 4181 (see Fig. 10) under controlled conditions.

5. Results

5.1. Laboratory results

Fig. 11 shows the temperature for both connectors, C1 and C2, in function of current considering two different conditions, regular (Fig. 11a) and coated (Fig. 11b) surfaces. Vertical bars denote uncertainty ranges for a 95% of confidence level. As shown in Fig. 11a, connectors C1 and C2 present uncertainties close to ±80 K and ±70 K for a 450 A electrical current. This result contradicts the affirmation that thermography accuracy improves in inspections of deteriorated connectors. Fig. 11a also shows that for 150 A, 200 A, 250 A, 300 A, 350 A and 400 A, the temperature uncertainty intervals of connectors C1 and C2 partially overlap. Under the metrological point of view, this particular result indicates that is not possible to guarantee a temperature distinction (neither deterioration stage) between both connectors at these electrical current values, which is an incorrect conclusion since C1 is highly degraded and C2 has not been used before.

On the other hand, coated regions at the connectors C1 and C2 present low uncertainty intervals, with approximately ±9 K and ±8.5 K, respectively, for 450 A electrical current value, as shown in Fig. 11b.

5.2. Infrared thermographic inspection in an electrical substation

We also performed an outdoor thermographic inspection in electrical connectors of a substation to exemplify the drawbacks of using comparative methods for decision making.

Two electrical disconnectors (A and B) are shown in Fig. 12. At the ends is possible to identify conductor cables and electrical connectors that link the equipment to the system. Disconnector A is being evaluated, whereas disconnector B is the reference. We measured temperature in two points for each component, T_{p1} and T_{p2} for disconnector A, T_{ref1} and T_{ref2} for disconnector B. The subscripts 1 and 2 mean cable and connector, respectively.

In a first analysis, we considered an emissivity of 0.75, which is an arbitrary value usually chosen for inspections in Brazil. After, we considered the emissivity of rusty aluminum $\varepsilon = 0.30$, obtained from the literature [17], to enrich the discussion.

Table 5 shows the temperature measurements T_p, T_{ref} and ΔT_{ref} evaluated by GUM and MCM, considering the emissivity of 0.75. ΔT_{ref2} value is 15.2 K with confidence level from 13.2 K to 17.3 K. Using NETA standard (see Table 1) as reference ΔT_{ref2} might be considered, simultaneously, as "repair as time permits" (4 °C–15 °C), and as "replace immediately" (>15 °C), leading to an ambiguous conclusion.

If emissivity is 0.30, as shown in Table 6, temperature rises 11% and 8.2% in terms of T_{p1} and T_{p2}, respectively, and uncertainty

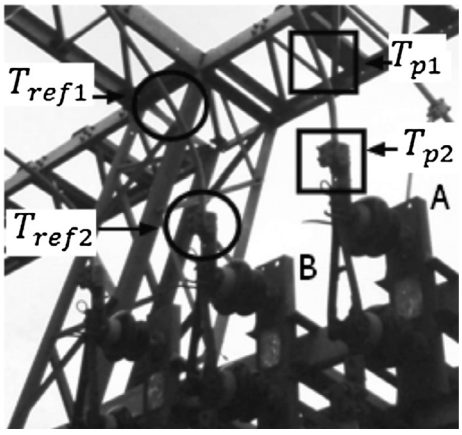

Fig. 12. Thermography inspection in electrical substation.

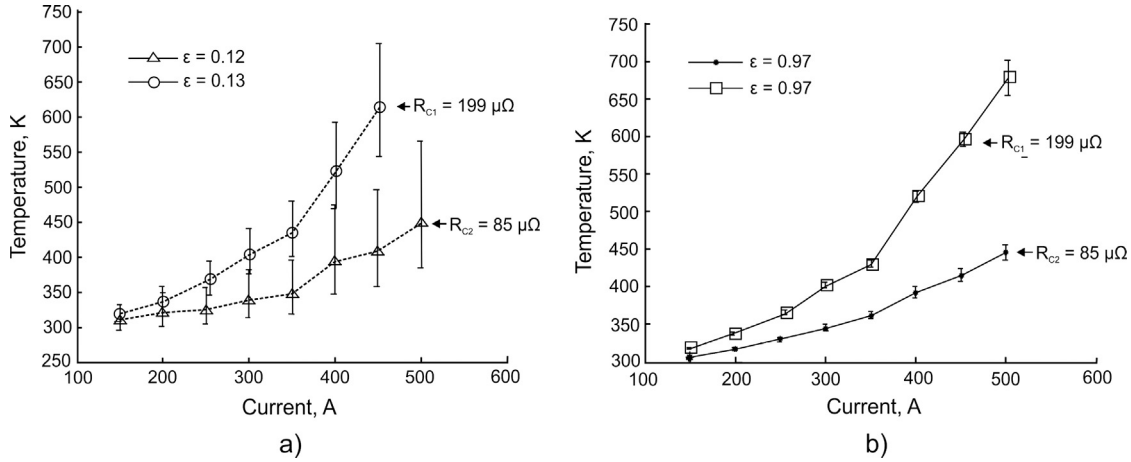

Fig. 11. Temperature and electrical current relation for a) C1 ($\varepsilon = 0.13$) and C2 ($\varepsilon = 0.12$) b) C1 and C2 ($\varepsilon = 0.97$).

Table 5
T_p, T_{ref} and ΔT_{ref} results for points 1 and 2 using $\varepsilon = 0.75$ (see Fig. 12).

Method	T_{ob}, K	$u(T_{ob})$, K	Confidence (95%)	d_{low}	d_{high}	Method	T_{ob}, K	$u(T_{ob})$, K	Confidence (95%)	d_{low}	d_{high}
T_{p1}						T_{p2}					
GUM	329.7	1.3	[327.3 332.2]	0.1	0.0	GUM	319.4	1.0	[317.5 321.2]	0.2	0.1
MCM	329.7	1.3	[327.4 332.2]			MCM	319.4	0.9	[317.7 321.2]		
T_{ref1}						T_{ref2}					
GUM	301.2	0.5	[300.3 302.2]	0.1	0.1	GUM	304.2	0.5	[303.1 305.2]	0.1	0.1
MCM	301.2	0.6	[300.2 302.3]			MCM	304.2	0.5	[303.2 305.1]		
ΔT_{ref1}						ΔT_{ref2}					
GUM	28.5	1.4	[25.9 31.2]	0.0	0.1	GUM	15.2	1.1	[13.1 17.4]	0.2	0.1
MCM	28.6	1.4	[25.9 31.3]			MCM	15.2	1.1	[13.2 17.3]		

Table 6
T_p, T_{ref} and ΔT_{ref} results for points 1 and 2 using $\varepsilon = 0.30$ (see Fig. 12).

Method	T_{ob}, K	$u(T_{ob})$, K	Confidence (95%)	d_{low}	d_{high}	Method	T_{ob}, K	$u(T_{ob})$, K	Confidence (95%)	d_{low}	d_{high}
T_{p1}						T_{p2}					
GUM	365.7	5.3	[355.4 376.2]	2.1	0.2	GUM	345.2	4.0	[337.4 353.3]	1.1	0.2
MCM	366.2	5.4	[357.5 376.0]			MCM	345.5	4.1	[338.5 353.1]		
T_{ref1}						T_{ref2}					
GUM	305.3	1.6	[302.3 308.4]	0.6	0.8	GUM	312.3	1.9	[308.7 316.0]	0.2	0.7
MCM	305.4	1.9	[301.8 309.2]			MCM	312.4	2.1	[308.5 316.6]		
ΔT_{ref1}						ΔT_{ref2}					
GUM	60.5	5.2	[49.6 71.3]	1.3	0.2	GUM	32.9	4.4	[24.3 41.4]	0.4	0.6
MCM	60.8	5.7	[50.9 71.4]			MCM	33.1	4.6	[19.2 42.0]		

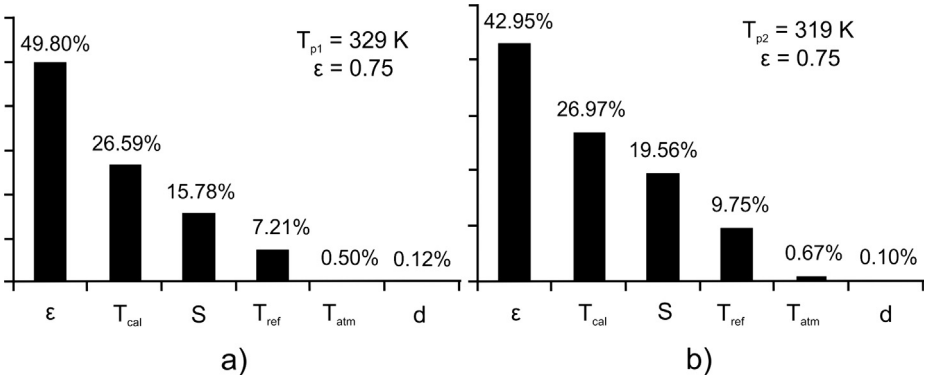

Fig. 13. Source of uncertainty contributions (a) T_{p1} and (b) T_{p2} of disconnector A considering $\varepsilon = 0.75$.

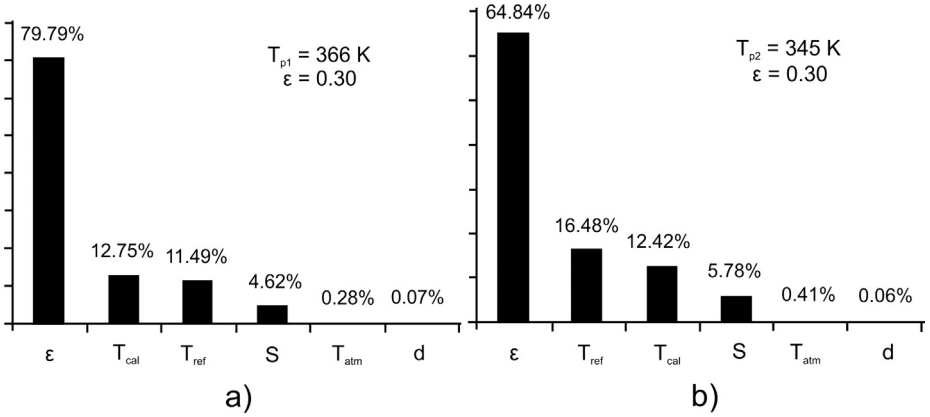

Fig. 14. Source of uncertainty contributions (a) T_{p1} and (b) T_{p2} of disconnector A, considering $\varepsilon = 0.30$.

increases critically. In both cases ($\varepsilon = 0.30$ or 0.75), we recommend to analyze the sources of uncertainty separately, looking to a better diagnosis.

Fig. 13 shows the contributions of each uncertainty source for T_{p1} and T_{p2}, considering $\varepsilon = 0.75$. In both T_{p1} and T_{p2}, the surface emissivity is responsible for up to 40%, and atmospheric temperature and target distance are not representative. Fig. 14 shows the same analysis for the emissivity of 0.30. It is possible to see that for a lower emissivity values its contribution to uncertainty becomes even more significant. Additionally, regarding the numerical tolerance (see Table 6), GUM shows to be ineffective for the emissivity of 0.30 ($|d_{high} - d_{low}| \geqslant \delta$), providing a low quality confidence level.

6. Conclusions

In this article we applied uncertainty analysis to the results of thermographic inspections in electrical connectors during tests in laboratory and outdoor conditions. Using GUM and MCM methods, we demonstrate the high influence that emissivity has on temperature uncertainty intervals, especially in low emissivity surfaces.

A test bench was mounted to simulate operational conditions of electrical connectors and we performed thermographic inspections in steady-state conditions for two H-type connectors in very different degradation levels. We could conclude that the uncertainties intervals partially overlap at a wide range of current values in the non coated surfaces during the tests. This result contradicts the affirmation that thermography accuracy improves in inspections of deteriorated connectors.

As expected, emissivity impacts the temperature uncertainty highly, reinforcing the fact that adopting emissivity values without any scientific support is not a recommended practice. In case of low emissivity surfaces, the outdoor inspection indicated that the results accuracy was compromised due to the high uncertainty involved, and comparative methods may lead to incorrect diagnosis.

Uncertainty sources other than emissivity did not represent a great influence on the results accuracy, in special atmospheric temperature and target distance, considering the experiments performed. Regarding the method to determine uncertainty, Monte Carlo Method (MCM) shows to be more appropriate than GUM, mainly for low values of emissivity. In this case, GUM does not meet the criteria established by the Joint Committee for Guides in Metrology.

Acknowledgement

This project was supported by P&D 426 ANEEL (Agência Nacional de Energia Elétrica). The authors gratefully acknowledge the financial support received from CNPq and CAPES.

References

[1] ANSI/NETA MTS, Standard for Maintenance Testing Specifications for Electrical Power Equipment and Systems, International Electrical Testing Association, 2011.
[2] A. Ferrero, M. Prioli, S. Salicone, The construction of joint possibility distributions of random contributions to uncertainty, IEEE Trans. Instrum. Meas. 63 (1) (2014) 80–88.
[3] A. Taheri-Garavand, H. Ahmadi, M. Omid, S.S. Mohtasebi, K. Mollazade, A.J.R. Smith, G.M. Carlomagno, An intelligent approach for cooling radiator fault diagnosis based on infrared thermal image processing technique, Appl. Therm. Eng. 87 (2015) 434–443.
[4] R. Morello, Potentialities and limitations of thermography to assess landslide risk, Measurement 116 (2018) 658–668.
[5] F. Wang, Y. Wang, J. Liu, Y. Wang, Theoretical and experimental study on carbon/epoxy facings-aluminum honeycomb sandwich structure using lock-in thermography, Measurement 126 (2018) 110–119.
[6] C.M. Basheer, C.V. Krishnamurthy, K. Balasubramaniam, Hot-rod thermography for in-plane thermal diffusivity measurement, Measurement 103 (2017) 235–240.
[7] C. Capua, R. Morello, I. Jablonski, Active and eddy current pulsed thermography to detect surface crack and defect in historical and archaeological discoveries, Measurement 116 (2018) 676–684.
[8] P.R. Muniz, R.A. Kalid, S.P.N. Cani, R.S. Magalhães, Handy method to estimate uncertainty of temperature measurement by infrared thermography, Opt. Eng. 53 (7) (2014) 074101.
[9] W. Minkina, S. Dudzik, Simulation analysis of uncertainty of infrared camera measurement and processing path, Measurement 39 (8) (2006) 758–763.
[10] K. Chrzanowski, R. Matyszkiel, J. Fischer, J. Barela, Uncertainty of temperature measurement with thermal cameras, Opt. Eng. 40 (6) (2001) 1106–1114.
[11] M. Musto, G. Rotondo, M. Cesare, A. Del Vecchio, L. Savino, F. Filippis, Error analysis on measurement temperature by means dual-color thermography technique, Measurement 90 (2016) 265–277.
[12] M.S. Jadin, S. Taib, Recent progress in diagnosing the reliability of electrical equipment by using infrared thermography, Infrared Phys. Technol. 55 (4) (2012) 236–245.
[13] A.S.N. Huda, S. Taib, Application of infrared thermography for predictive/preventive maintenance of thermal defect in electrical equipment, Appl. Therm. Eng. 61 (2) (2013) 220–227.
[14] M.A. Mendes, L.G.R. Tonini, P.R. Muniz, C.B. Donadel, Thermographic analysis of parallelly cables: a method to avoid misdiagnosis, Appl. Therm. Eng. 104 (2016) 231–236.
[15] A.S.N. Huda, S. Taib, Suitable features selection for monitoring thermal condition of electrical equipment using infrared thermography, Infrared Phys. Technol. 61 (2013) 184–191.
[16] B.P.A. Silva, R.A.M. Ferreira, S.C. Gomes Jr., F.A.R. Calado, R.M. Andrade, M.P. Porto, On-rail solution for autonomous inspections in electrical substations, Infrared Phys. Technol. 90 (2018) 53–58.
[17] FLIR Systems, User's manual FLIR B6XX series FLIR P6XX series FLIR SC6XX series, Number 1558550 in 1st ed., FLIR, 2010.
[18] Joint Committee for Guides in Metrology, JCGM 200: 2012 International Vocabulary of Metrology Basic and General Concepts and Associated Terms, third ed., JCGM, 2012.
[19] W. Minkina, S. Dudzik, Infrared Thermography: Errors and Uncertainties, first ed., Wiley, 2009.
[20] P.M. Harris, M.G. Cox, On a monte carlo method for measurement uncertainty evaluation and its implementation, Metrologia 51 (4) (2014) S176–S182.
[21] C. Wang, Z. Qiu, Y. Yang, Uncertainty propagation of heat conduction problem with multiple random inputs, Int. J. Heat Mass Transf. 99 (2016) 95–101.
[22] Joint Committee for Guides in Metrology, Evaluation of Measurement Data Supplement 1 to The Guide to the Expression of Uncertainty in Measurement – Propagation of Distributions Using a Monte Carlo Method, first ed., JCGM, 2008.
[23] S. Tezuka, Uniform Random Numbers – Theory and Practice, Springer, US, 1995.
[24] K. Chrzanowski, Evaluation of thermal cameras in quality systems according to ISO 9000 or EN45000 standards, Proc. SPIE 4360 (2001) 387–401.
[25] International Organization of Legal Metrology, OIML R141: Procedure for Calibration and Verification of the Main Characteristics of Thermographic Instruments, OIML, 2008.
[26] B. Lehmann, K.G. Wakili, Th. Frank, B.V. Collado, Ch. Tanner, Effects of individual climatic parameters on the infrared thermography of buildings, Appl. Energy 110 (2013) 29–43.
[27] A. Kylili, P.A. Fokaides, P. Christou, S.A. Kalogirou, Infrared thermography (IRT) applications for building diagnostics: a review, Appl. Energy 134 (2014) 531–549.